Icarus 211 (2011) 1–9

Contents lists available at ScienceDirect

Icarus

journal homepage: www.elsevier.com/locate/icarus

Comet-like tail-formation of exospheres of hot rocky exoplanets: Possible implications for CoRoT-7b

A. Mura [a,*], P. Wurz [b], J. Schneider [c], H. Lammer [d], J.-M. Grießmeier [e], M.L. Khodachenko [d], J. Weingrill [d], E. Guenther [f,1], J. Cabrera [g], A. Erikson [g], M. Fridlund [h], A. Milillo [a], H. Rauer [g,i], Ph. von Paris [g]

[a] Istituto di Fisica dello Spazio Interplanetario – INAF, Via del Fosso del Cavaliere 100, 00133 Rome, Italy
[b] Physics Institute, University of Bern, CH-3012 Bern, Switzerland
[c] LUTH, Observatoire de Paris, CNRS, Université Paris Diderot, 92190 Meudon, France
[d] Space Research Institute, Austrian Academy of Sciences, 8042 Graz, Austria
[e] Netherlands Institute for Radio Astronomy, 7991 PD Dwingeloo, The Netherlands
[f] Thüringer Landessternwarte Tautenburg, Sternwarte 5 07778 Tautenburg, Germany
[g] Institut für Planetenforschung (DLR), Rutherford Street 2, 12489 Berlin, Germany
[h] RSSD, ESTEC, ESA, Keplerlaan 1, Postbus 299, 2200 AG Noordwijk, The Netherlands
[i] Technische Universität Berlin, D-10623 Berlin, Germany

ARTICLE INFO

Article history:
Received 2 December 2009
Revised 16 August 2010
Accepted 23 August 2010
Available online 27 August 2010

Keywords:
Extrasolar planets
Planetary formation
Atmospheres, Composition

ABSTRACT

In this study, the interaction of stellar wind plasma with the exosphere and possibly with the planetary magnetospheric environment of close-in rocky exoplanets is investigated. In particular, we focus on the "super-Earth" CoRoT-7b, which has been recently discovered by the CoRoT space observatory. The physical properties of such a planet, with an orbital distance of about 0.017 AU from its host star, may most likely resemble a big and more massive Mercury-type planet in the sense that it most likely releases its surface elements into space. Based on the present knowledge of CoRoT-7b and drawing on the analogy to Solar System planets, we use numerical models to simulate exospheric and magnetospheric distributions of different particle populations, among which are neutral sodium and ionised calcium and magnesium. We find that, for most species, the atmospheric loss rate in such an extreme environment can be very high, so that a neutral and an ionised tail of escaping particles will form. Depending on the planetary composition we postulate the presence of a sodium tail, similar to that of Mercury but shorter due to the shorter Na lifetime, and of an extended magnetospheric distribution of ionised calcium or magnesium. The feasibility of observation of such populations is also discussed.

1. Introduction

After the discovery of more than 400 giant exoplanets, the detection of increasingly smaller ("super-Earth") planets brought new interesting objects to investigate. The term "super-Earth" is a convention to designate planets with sizes from 1 R_{Earth} to 2 R_{Earth} and with masses up to 10 M_{Earth}.

In recent years, the detection and characterisation of giant exoplanets has made significant progress in the case where they are transiting their star allowing for the measurement of their radius. Different species in their atmosphere (H_2O, CH_4, CO_2, CO, Na) have been recently detected via spectroscopy during transits (e.g. Tinetti et al., 2007, and references therein). Here we investigate the possible gaseous environment of hot "super-Earth" planets (i.e., those very close to their parent star: $d < 0.045$ AU) and the consequence for transit spectroscopy. The idea of cometary tails of close-in extrasolar planets was first proposed by Schneider et al. (1998). Inspired by the case of the first discovered transiting super-Earth CoRoT-7b (Léger et al., 2009), we investigate the characteristics of exospheric tails of a super-Earth planet very close (~0.02 AU) to a solar-like star, with a very short orbital period (less than one day), assuming that it has a rocky surface and its host star is relatively young (2 Gyr). We use the physical and stellar parameters of CoRoT-7b as a proxy and note that the modelled scenarios and the obtained results should also be valid for similar type exoplanets.

CoRoT-7b has several remarkable features (see Section 2 and Table 1). Despite the very high temperature of the surface illuminated by its star of about 2500 K at the sub-stellar point, the atmospheric escape of low mass exospheric species (light volatiles like H, He, O, CH_4) through the Jeans mechanism is presently very limited since the escape speed at the exobase is 18.7 km s^{-1}, based on the mass and radius estimates given below. Even for hydrogen, the

* Corresponding author.
E-mail address: alessandro.mura@ifsi-roma.inaf.it (A. Mura).
[1] Instituto de Astrofísica de Canarias, La Laguna (Tenerife), Spain.

0019-1035/$ - see front matter © 2010 Elsevier Inc. All rights reserved.
doi:10.1016/j.icarus.2010.08.015

Table 1
CoRoT-7b quantities and simulation parameters.

Parameter	Symbol	Value	References
Planetary mass	M_p	4.8 ± 0.8 M_{Earth}	Queloz et al. (2009)
Planetary radius	R_p	1.68 ± 0.09 R_{Earth}	Léger et al. (2009)
Orbital distance	a	0.017	Queloz et al. (2009)
Na photo-ionisation lifetime	τ_{Na}	20 s	Huebner et al. (1992) (scaled)
		56 s	Fulle et al. (2007) (scaled)
Ca photo-ionisation lifetime	τ_{Ca}	4 s	Killen et al. (2005) (scaled)
Ca^+ photo-ionisation lifetime	τ_{Ca+}	10^3 s	Estimate
Mg photo-ionisation lifetime	τ_{Mg}	500 s	Huebner et al. (1992) (scaled)
Mg^+ photo-ionisation lifetime	τ_{Mg+}	5×10^4 s	Estimate

fraction of escaping particles is about 0.4% at 2500 K. However, if permanently evaporated or released surface elements build up a thin atmosphere (Schaefer and Fegley, 2009) and if the thermosphere is heated to even higher temperatures, then thermal escape could even result in hydrodynamic outflow and hence higher atmospheric loss rates. In any case, neutral particles that are released into space will soon be ionised and dragged away from the planet by the dense stellar wind plasma flow. Thus, a relevant process for exospheric escape is photo-ionisation, since the created ions become part of the magnetosphere (if there is any) and are picked up by the stellar wind.

Recent studies by Lammer et al. (2009) and Leitzinger et al. (2009) concluded that, depending on the initial density and mass, some escape scenarios allow that CoRoT-7b is the remnant of a low density "sub-Uranus"-type planet, but was most likely always a low mass rocky planet and not a core of a more massive larger object.

At present, the remaining rocks release volatiles and thermal decomposition products from their minerals into space at the day-side surface (Schaefer and Fegley, 2009). We expect that the stellar radiation pressure and the plasma environment will cause the build up of an elongated comet-like exosphere (coma), consisting of species which are released and evaporated from the surface minerals, with an unusually large tailward extension. In this study we simulate this elongated exosphere and apply the results to a potential spectroscopic investigation of this transiting coma, by absorption features during its transit in front of the star.

For a Solar System planet like Mercury, whose environment comes closest to planets like CoRoT-7b, the sodium exosphere and tail and the calcium exosphere were already observed from the ground (Potter et al., 2002; Bida et al., 2000; Schleicher et al., 2004) and during the Mercury flybys of the MESSENGER spacecraft (McClintock et al., 2009). Compared to Mercury, where the exosphere is bounded to the surface with a maximum temperature of about 700 K (see reviews by Killen and Ip (1999) and Killen et al. (2007)), the exobase of hotter and more extreme super-Earth planets is most likely located above a thin layer of a thermally evaporated atmosphere, and, for super-Earth planets at ~0.02 AU from a G-type star, the temperature is expected to be above 2500 K at the sub-stellar point.

At Mercury, the sodium neutral atom tail is formed by the strong radiation pressure, which pushes away some of the uppermost exospheric atoms in the anti-sunward direction (Ip, 1986; Potter et al., 2002), which is a well-known and studied process on Mercury (e.g., Smyth and Marconi, 1995). At super-Earth planets like CoRoT-7b so close to their star, the radiation pressure for Na is extremely high. By rescaling this force from Mercury orbit to 0.02 AU, the radiation pressure is at least one order of magnitude higher than the gravity acceleration. Since this force is tangential to the atmosphere layer at the termination regions, it happens that most of the Na atoms in the terminator region of the exosphere are rapidly accelerated toward the night side of the planet, forming a neutral Na atom tail, where the particles escape from the planet. Even if the UV radiation causes rapid ionisation of Na particles, because of the radiation pressure acceleration, and because of the higher Na flux provided by the higher density and temperature, the tail of neutral Na atoms in the anti-stellar direction is predicted to be much more intense at a hot super-Earth planet than at Mercury, where the Na densities in the tail region are observed to be orders of magnitude lower than in Mercury's day-side exosphere (Potter et al., 2002).

In addition, due to the extremely intense stellar wind particle flux, protons are likely to impact the uppermost exosphere layer. Such protons can produce energisation of neutral exospheric particles, known as atmospheric sputtering (e.g., Johnson, 1990; Lammer and Bauer, 1993) and hence increase the intensity of the neutral tail.

Neutral calcium in the exosphere is very rapidly ionised by stellar UV. Such Ca ions are picked up by the stellar wind, dragged in the anti-star direction, and also form a tail, in this case an ion tail. Depending on the presence of a significant dipole magnetic field of the planet, such an ion tail is either confined inside a magnetosphere (if the body has a magnetic field able to form one) or is embedded in the stellar wind itself.

While the direction of the sodium atom tail is dictated by the radiation pressure and hence is in the anti-stellar direction, the ionised calcium tail is in the direction of the stellar wind. Because of the high orbital velocity of a planet located in a ~0.02 AU orbit, the stellar wind has an aberration of about 45° when viewed from the planet. Hence, such an ion tail may be easier to detect, which is discussed below.

It is expected that close-in extrasolar planets are synchronously rotating with their host star because of the strong tidal interaction. For gravitationally locked planets the rotation period is equal to the orbital period, which is usually much longer than the rotation period expected for planets not subject to tidal locking. However, the orbital period of super-Earth planets like CoRoT-7b (22 h, in that case) may be comparable or even shorter than the rotation period of the Earth. Several studies, like Khodachenko et al. (2007) and Grießmeier et al. (2009), expect from dynamo scaling models that the slower rotation of these planets results in relatively small magnetic moments. On the other hand, such scaling is debated, since other authors (e.g. Christensen and Aubert, 2006) claim that magnetic field generation and strength are independent of planetary rotation rate. Incidentally, because the planetary revolution period of the planet is very close to that of the Earth, both approaches lead to the same magnetic moment in the case of CoRoT-7b. In any case, since the Ca^+ tail is confined inside the magnetosphere of the planet, if there is any, the distribution of Ca^+ reflects the magnetospheric configuration. Hence the observation of Ca^+ would provide some information on the magnetosphere of such planet. Since, in general, features like plate tectonics and magnetic dynamo activity are highly debated for super-Earths (e.g. O'Neill et al., 2007; Valencia et al., 2007), detection of such a magnetic field would be extremely helpful in studying the interior of super-Earth planets and magnetic dynamo generation in general.

2. Models of CoRoT-7b-like exospheres

CoRoT-7b is the first super-Earth planet with a measured radius, 1.68 R_{Earth} (Léger et al., 2009); its mass is 4.8 ± 0.8 M_{Earth} (Queloz

et al., 2009; see Table 1 for a list of related physical quantities). As discussed before, the observational parameters indicate that CoRoT-7b is definitely the first rocky exoplanet. It is extremely close to its parent G8 V star ($R_{star} = 0.93\ R_{Sun}$, $T_{star} = 5275$ K), at only 0.017 AU, i.e., the orbit radius is only 4.1 times the stellar radius. The stellar age is estimated to be between 1.3 and 2.3 Gyr (Léger et al., 2009). As we show later, the planet rotation is synchronised with the orbital period of only 0.85 days (producing a planetary transit every day). The temperature at the sub-stellar point can be estimated, using the Stefan–Boltzmann law, to be about 2500 K.

The measured radius R_{pl} is 1.68 R_{Earth}, which is the smallest radius ever measured for an exoplanet. In principle there can be a significant contribution to this measured (total) radius by a thick extended hydrogen atmosphere (Adams et al., 2008; Grasset et al., 2009), amounting up to 60% of the total radius. For such cases the core radius is expected to be between 0.7 and 2 R_{Earth}. However, some values of (M, R) are excluded by the Grasset et al. (2009) model. In particular the lower limit of 0.8 R_{Earth} falls well below the theoretical lower limit of 5 M_{Earth} for a planet without water given by Grasset et al. (2009) for a 10 M_{Earth} planet. From this value we can already infer that for a mean value mass of about 5 M_{Earth} there should be no thick extended hydrogen atmosphere. This assumption is also supported by recent atmospheric mass loss model results that indicate the CoRoT-7b should have lost its initial hydrogen envelope (Lammer et al., 2009; Leitzinger et al., 2009).

According to these studies, a hot super-Earth planet with the range of parameters of CoRoT-7b is most likely not a remaining core of a hot Jupiter that lost its hydrogen atmosphere. Both works study the thermal evaporation of hydrogen-rich exoplanets by applying a mass loss formula which includes Roche Lobe effects, heating efficiencies, etc. and are in agreement with hydrodynamic model results during evolutionary epochs (Penz et al., 2008). Leitzinger et al. (2009) placed virtual exoplanets with the size and mass of discovered gas giants and Neptune-class planets at ~0.02 AU from the star (approximately the location of CoRoT-7b) and modelled the mass loss, which indicates that hydrogen-rich gas giants within the mass domain of Saturn or Jupiter cannot lose enough mass so that a 5 M_{Earth} planet like CoRoT-7b remains as a residue. Furthermore, their results indicate that the mass of CoRoT-7b cannot be obtained by the thermal evaporation of the hydrogen envelope of a Neptune or Uranus-class object during 5 Gyr. They conclude that, depending on the initial density and mass, some escape scenarios show that CoRoT-7b could probably be the remnant of a low density "sub-Uranus"-type planet, but was most likely always a low mass rocky planet and not a core of a more massive larger object. Because one can expect that CoRoT-7b lost also its out-gassed volatiles from the primordial atmosphere the planet appears to be more like a "super-Mercury" under much extremer environmental conditions. Light exospheric species like hydrogen within CoRoT-7b's environment will have their origin most likely in the dense stellar wind.

In absence of precise knowledge of the surface and thermally out-gassed secondary atmospheric composition of this type of planets, we have arbitrarily assumed two cases for a surface composition of the planet. The first case resembles that of Mercury, which contain a Na and Ca surface fraction of 1.34% and 1.67%, respectively (e.g. Wurz et al., 2010). On the Moon, the average Na and Ca fractions are 0.31% and 4.6% (Wurz et al., 2007). In a second case it is expected that CoRoT-7b is a Mercury-type rocky planet but with a composition (density) which is closer to that of the Earth (Schaefer and Fegley, 2009). Schaefer and Fegley (2009) applied the MAGMA code of Fegley and Cameron (1987) to model the composition of silicate atmospheres which are produced by the vaporisation of volatile-free Earth-like super-Earth's. Their model calculations indicate volatile elements such as H, C, N, S, and Cl have been lost from the planet, but find that the silicate atmospheres which are composed primarily of Na, O_2, O, Mg and SiO gas could sustain (Schaefer and Fegley, 2009). The major compounds in our second case are most likely O, Mg and SiO. More realistic values for these quantities may be obtained once more observations are performed.

2.1. A neutral atmosphere around planets like CoRoT-7b?

The exobase density n_{exo} for the various components can be estimated from the standard physical approach, assuming that the mean free path l is equal to the scale height H;

$$n_{exo} = (mg)/(kT_{exo}\sigma_c), \quad (1)$$

where m is the particle mass, g the gravitational acceleration at the exobase level, k the Boltzmann constant, T_{exo} the exobase temperature, and σ_c the collision cross section. By using accurate values for the above mentioned quantities, the density is found to be about 6×10^{11} m^{-3} for Ca, 6×10^{12} for Mg, and 1.5×10^{11} m^{-3} for Na atoms.

We calculate the vertical density profiles for various possible volatile species such as H, H_2, He, CH_4, CO_2 and refractory species Si, Ca, Na in the exosphere, by assuming vapour pressure equilibrium at the surface and transport to the exobase. The calculations are done using a Monte-Carlo code (Wurz and Lammer, 2003) assuming an exobase at 200 km with a temperature of 2500 K, being the same as the surface temperature at the star-illuminated side (Léger et al., 2009). Despite this high temperature, Jeans escape is negligible because of the high escape speed at the exobase. Also the scale heights are in the range of 10–200 km (depending on the particle mass). The major escape channel from the exosphere is via photo-ionisation since the formed ions become part of the magnetosphere or of the stellar wind. For CoRoT-7b, the ionisation fractions, as derived from the model calculation (see Wurz and Lammer, 2003), for the considered species are: H 18.9%, H_2 10.8%, He 6.1%, CH_4 21.6%, CO_2 21.3%, and for the elements of mineral origin they are: Si 66.4%, Na 94.1%, Ca 99.5%. Ionisation rates are from Huebner et al. (1992), for Na and Mg from Fulle et al. (2007), and for Ca from Killen et al. (2005), adapted to the situation at CoRoT-7b, are used for this calculation. The radiation pressure acceleration is not computed here; in fact, for Calcium, the exobase density (6×10^{11} m^{-3}) multiplied by the atmosphere height (200 km) is much bigger than the inverse of the adsorption cross section, and we assume that the atmosphere is not optically thin.

Tian et al. (2009) investigated the response of the Earth's present atmosphere to extreme solar EUV conditions and found that the exobase level, which separates the collision dominated atmosphere from the collision-less of an Earth-mass planet with the present Earth's atmospheric composition, would rapidly hydrodynamically expand. In Tian et al. (2009) the exobase level for a nitrogen atmosphere would rise for an EUV flux that is 10 times that of the present Sun in 1 AU from 500 km up to about 5 Earth-radii. Such an expansion is highly depended on the atmospheric composition, in particular on the availability or absence of IR-coolers and the mass of the planet. Kulikov et al. (2006) showed that even a "dry Venus" with the present 96% CO_2 atmosphere the exobase would expand from 200 km up to about 1500 km altitude if Venus' atmosphere would be exposed by a 100 times higher EUV flux than at present. Because CoRoT-7b is about five times more massive compared to Earth or Venus, due to its higher g, even if one assumes that the thermosphere is heated up to 10,000 K, a rough estimation shows that its exobase level of its evaporated surface elements may not expand much higher than 1 planetary radius; Tian et al. (2009) however, showed that, if the atmosphere is rich in CO_2, the exobase level could be high. It is beyond the scope of this article to model in detail possible atmospheres, their EUV-induced expansion and related exobase levels. As a first approach,

we assume two different cases: one which has an exobase close to its surface at an altitude of 200 km, with temperature of 2500 K, and one extreme case where we assume that the exobase forms at 1 planetary radius, and the temperature is 10^4 K.

2.2. Neutral elongated exospheres

The 3D spatial distribution of a neutral exospheric component is obtained by using a Monte-Carlo single-particle model as in Mura et al. (2007). We use a coordinate system where x is from the centre of the planet towards the star, y is parallel to the orbital motion, z completes the right-handed reference frame. For a given source process, we define also the surface S from where we start tracking particles, which can be, for example, the planetary surface, the exobase or the magnetopause (for stellar wind protons). Then we launch a large number N_{tp} of test particles (N_{tp} is ~106 in this study). For each test particle, we randomly choose a starting point P_0 on S, and the starting velocity $\mathbf{v}_0$, according to the velocity distribution function. A weight w is associated to the test particle, which takes into account the number of real particles that it represents:

$$w(0) = \frac{A_s}{N_{tp}} \Phi_0, \tag{2}$$

where Φ_0 is the neutral particle flux generated at P_0, and A_S is the area of S. Then, the trajectory of the test particle is computed using the classical equation of motion, including gravity force, radiation pressure and non-inertial accelerations (i.e., Coriolis force). We numerically evaluate the time that test particles spend inside each grid cell, from which we can calculate the number density:

$$\frac{\partial n}{\partial E} = \frac{\sum_{i=1}^{N} w_i \Delta t_i}{dx\,dy\,dz\,dE}, \tag{3}$$

where Δt is the time elapsed inside the cell. The grid system has the shape of a rectangular box and is uniform; the number of grid points varies through simulation runs, and is of the order of $100 \times 50 \times 50$. Photo-ionisation does not actually remove test particles, it just decreases w in the simulation:

$$\frac{dw}{dt} = w(t) \sum_i \frac{1}{\tau_i}, \tag{4}$$

where τ_i is the photo-ionisation lifetime.

The photo-ionisation lifetime (τ) for sodium is calculated considering that $\tau = 6.25 \times 10^4$ s in Earth orbit (Huebner et al., 1992; however, Fulle et al. (2007), report a longer lifetime of 1.9×10^5 s). Since τ is inversely proportional to the photon flux, and assuming as a first guess that the host star has a spectrum similar to that of the Sun, τ_{Na} is about 20 s. For Ca, similar estimations give τ_{Ca} of about 4 s. The photo-ionisation process Eq. (4) and the radiation pressure force are not computed in the shadow of the planet. With the planet being located very close to the star (~4 R_S), the volume of complete shadow is a cone with the base at the planet terminator, and the vertex at $(-4, 0, 0)$ R_P.

2.3. Source processes

The uncertainties about the physical parameters to use in the simulations suggested us to perform different simulations related to different possible scenarios. For Na and Ca we consider two processes for release into the exosphere: thermal release from the exobase and atmospheric sputtering by stellar wind protons.

To calculate the spatial distribution of Ca^+ we assumed two magnetospheric configurations, namely (a) a completely non-magnetised body and (b) a body with a dipole magnetic field that is able to form a shielding magnetosphere. The results from both configurations will be compared below.

In the thermal release model, test particles are randomly generated at the exobase with a Maxwellian law, using a uniform exobase temperature from 2500 K to 10,000 K.

Atmospheric sputtering is the release of atmospheric particles due to multiple scattering of high-energy solar wind ions onto atmospheric thermal neutral particles (Lammer and Bauer, 1993). Here, a simplified atmospheric model of H, H_2, CO, CO_2 and Na is used. A stellar wind proton flux of 5×10^{12} cm^{-2} s^{-1} is assumed by scaling the solar wind parameters from Mercury orbit (v = 450 km/s, n = 60 cm^{-3}) to 0.017 AU, taking also into account a stellar age of 2 Gyr, which is in between the suggested range of 1.2 and 2.3 Gyr that can be inferred from spectral observations (Léger et al., 2009). The proton mean velocity and temperature are extrapolated from solar wind as well. Test particles are launched and tracked until they collide with the surface. Na atoms, energised by this process, are able to escape the planet's gravity field and, thanks to the radiation pressure, form a Na tail.

The exosphere of neutral Ca and Mg is simulated like the Na one, assuming thermal release from the exobase. The photo-ionisation lifetime of Ca in the exosphere of CoRoT-7b can be estimated by rescaling the solar flux to 0.017 AU, and is found to be about 4 s.

The ionised Ca and Mg particles are trapped inside the magnetosphere and magnetotail, which are modelled in two different ways as described before. Because of the high number of unknown parameters, we have adopted two simplified approaches: in the "non-magnetised body" model, newly created ions are picked up by the stellar wind, with same velocity and temperature, and dragged away from the planet. In the tail, these singly ionised atoms can be further ionised by the strong photon field. The ionisation lifetime for Ca^+ is roughly estimated by considering that the second ionisation potential (11.871 eV) is about twice the first ionisation potential (6.1132 eV), and that the photon flux above that threshold is less than 1% of that above 6 eV. Hence, the Ca^+ lifetime in the tail is estimated as 10^3 s. In the "magnetised-body" case, the Ca^+ ions circulate inside an assumed Mercury-like magnetosphere, which also includes a magnetotail, until the photo-ionisation process renders them doubly ionised and they are not accessible for our observation anymore. For Mg, with similar consideration about first and second ionisation potentials (~7 eV, ~15 eV), we estimate the second ionisation lifetime of the order of 5×10^4 s.

The global loss rate for exospheric thermal release of Na can be estimated as $Q = 4\pi R_{pl}^2 n v$, where n is the exosphere density and v is the mean particle velocity at the exobase. In the most extreme case where the stellar wind impacts directly onto the surface and it is not deviated by the magnetic field, the global loss rate is given by ion sputtering, which is $Q' = 4\pi R_{pl}^2 n_{sw} v_{sw} Y c_{Na}$, where n_{sw} is the stellar wind density, v_{sw} is the stellar wind velocity, Y is the ion sputtering yield and c_{Na} is the surface fraction of sodium. Using the parameters in the manuscript, and also taking v = 1000 m/s (for T = 2500 K), Y = 0.05, c_{Na} = 0.53% (as at Mercury), we obtain $Q \sim 10^{29}$ s^{-1}, $Q' \sim 10^{27}$ s^{-1}. Hence, in the case of an airless body, the sodium tail should be a factor 100 less dense than in this study.

2.4. Planet synchronisation

To discuss the temperature distribution on the planet, it is important to know whether its rotation is synchronised or not with its orbital revolution by tidal locking. From the definition of the Love number $k2$ in Gladman et al. (1996) and their formula for the time of tidal locking, we have (Grießmeier et al., 2009):

$$t_{lock} \approx \frac{4}{9} \alpha Q'_p \left(\frac{R_p^3}{G M_p} \right) (\omega_i - \omega_f) \left(\frac{M_p}{M_*} \right)^2 \left(\frac{d}{R_p} \right)^6, \tag{5}$$

where M_p is the planet mass (4.8 M_E), M^* is the mass of the host star, R_p is the planet radius (1.68 · R_E), Q' is a parameter (500), ω_i is the initial rotation rate (assuming an initial rotation period between 13.1 h and 30 h, lower and upper limits), ω_f is the actual rotation rate, $\alpha = 0.33$; d is the semi-major axis of the motion of the planet around the star, G is the gravitational constant; the choice of Q'_p, ω and α is described in Grießmeier et al. (2009); all units are in CGS. This is valid assuming uniform density in the planet; however, note that according to some authors this scenario may not occur at super-Earths planets (i.e., Valencia et al., 2007).

We then find t_{lock} between 3.9 and 9.0 years for a rocky planet. Compared to the assumed stellar age of 1.2–2.3 Gyr (Léger et al., 2009), we can safely conclude that for any reasonable value of ω, Q and α the planet rotation is synchronised with its orbital period. Fig. 1 shows tidally locked versus freely rotating regime for "super-Earth" planets of 4.8 M_{Earth} as a function of orbital distance d and mass M^* of the host star.

2.5. Magnetosphere

The value of the intrinsic magnetic field, if any, is presently unknown. Hence, the configuration of the magnetosphere is not known either. However, one can calculate the minimum value of the intrinsic magnetic field, which would be able to sustain a magnetopause. At the stand-off point, r_{so}, the pressure balance between the plasma pressure of the stellar wind (left-hand side) and the magnetic field pressure (right-hand side) is:

$$\rho v^2 = \frac{4}{2\mu_0}\left(\frac{M}{r_{so}^3}\right)^2, \tag{6}$$

where ρ and v are the stellar wind mass density and bulk velocity, M is the dipole momentum in units of T m^3, μ_0 is the magnetic constant $4\pi \times 10^{-7}$ (Walker and Russel, 1995; Grießmeier et al., 2005), this can be used to evaluate the stand-off distance r_{so} as a function of the magnetic dipole moment M (see Fig. 2).

It appears that, if the planet had a magnetic moment like the Earth ($M = 8 \times 10^{15}$ T m^3), it would have an extremely small magnetosphere like Mercury, where the stand-off distance is about 1.5 planetary radii, and to have a magnetosphere comparable to that of the Earth (stand-off at about 10 planetary radii), it should have a magnetic moment like Jupiter. The latter is very unlikely, also because the planet is tidally locked to the host star. Hence, in this study we consider two cases: a non-magnetised with no intrinsic magnetosphere; and a magnetised body with a magnetosphere with a size similar to that of Mercury, rescaled to have the same value of r_{so} (≈1.5) in planetary radii units. The planet orbits at 0.017 AU from its host star; the orbital period is 22 h. Hence, the orbital velocity of the planet is about 200 km/s. This is the same

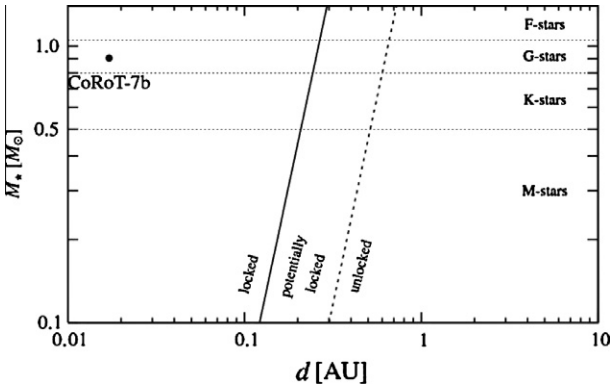

Fig. 1. Tidally locked (left) versus freely rotating (right) regime for "super-Earth" planets as a function of orbital distance d and mass M^* of the host star. The position of CoRoT-7b in this parameter space is indicated.

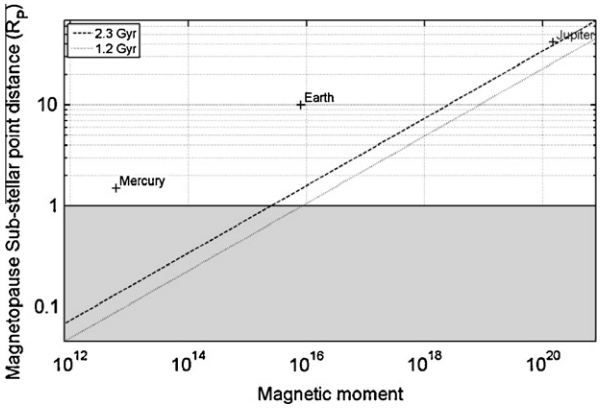

Fig. 2. Estimated magnetospheric sizes for different values of the planetary intrinsic magnetic moment, in (T m^3), for two stellar ages (1.2 and 2.3 Gyr). The horizontal line at 1 is the planetary surface, so the shaded area denotes cases in which the planet is not shielded from the stellar wind. Present time cases of Mercury, the Earth and Jupiter are plotted (crosses). For each planet, stand-off distance unit is the respective planetary radius. Even for a magnetic moment like that of the Earth, magnetosphere would be smaller than that of Mercury.

value as the expected stellar wind velocity at the planet's orbit, so when viewed from the planet the stellar wind with an aberration angle of about 45°. The magnetosphere of such planet should be tilted of the same angle. In the case of the magnetised body, it is likely that several magnetospheric current systems may form. The magnetosphere model used here does not include them, since the present knowledge of the planet does not allow reconstructing them in detail. However, similarly to Mercury's case, only a Harris current sheet is included, as in Delcourt et al. (2003).

2.6. Radiation pressure acceleration

The radiation pressure acceleration a_r originates from the momentum transfer of photons via the absorption lines of the neutral species. For Na and K, such effect sometimes needs to be taken into account in planetary environments. At Mercury, as an example, the Na acceleration can be up to 54% of the surface gravity, ranging between 0.2 and 2 m/s^2 (Potter et al., 2002). The radiation pressure for Ca is about a factor 4 less than that of Na (McClintock et al., 2009), and because of the very short ionisation lifetime, radiation pressure does not play an important role for Ca.

In general, this acceleration is proportional of the photon flux and, hence, is expected to be extremely high at super-Earth planets like CoRoT-7b. For Na, more specifically, the acceleration depends also on the amount of Doppler shift out of the Fraunhofer features (for a detailed discussion, see Smyth and Marconi, 1995; Potter et al., 2002), so that the acceleration increases as the radial velocity of the particle with respect to the star increases. In the case of Mercury, the planet radial velocity (due to orbit eccentricity) plays an important role. For CoRoT-7b we assume a circular orbit, and the radial velocity of the reference frame is zero. Barnes et al. (2010) discussed orbital eccentricity and tidal heating of CoRoT-7b and -7c in detail consider tidal damping strong enough to circularise the planet orbits. In this study we estimate the radiation pressure for Na by rescaling the model already used at Mercury (Mura et al., 2009). For neutral Hydrogen, we have assumed a similar model, using data from Bzowski (2008). In the model, we calculate the Doppler shift as a function of each particle's velocity for each step in the particle trajectory calculation, and then we calculate the acceleration a_r. Fig. 3 shows the radiation pressure acceleration function of the radial velocity for H, Na and K; gravity and Coriolis accelerations are shown also, for comparison. It is evident that, in optically thin regions of the exosphere, where the stellar photon flux is unreduced, the radiation pressure acceleration is

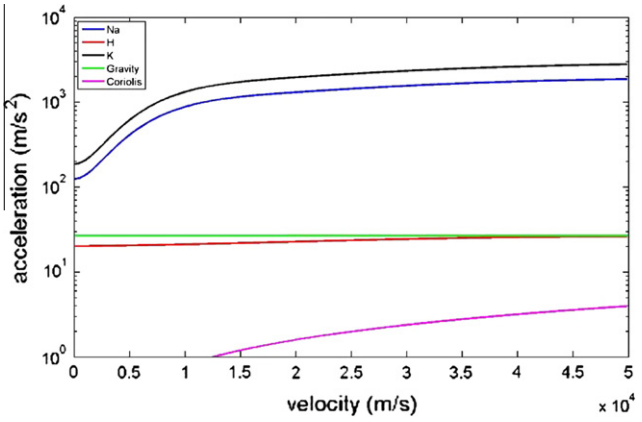

Fig. 3. Blue, red and black lines: radial radiation pressure acceleration for different neutral species, as estimated at CoRoT-7b, as a function of the particle radial velocity respect to the star. Green line: module of the gravity acceleration at the planetary surface. Magenta line: module of the Coriolis acceleration, as a function of the velocity. (For interpretation of the references to colour in this figure legend, the reader is referred to the web version of this article.)

considerably higher than the gravity acceleration for Na and Ca, and comparable for H. In the sub-solar regions, the radiation pressure pushes the exosphere closer to the planet; in the terminator regions, it is able to accelerate Na and Ca atoms tailwards to form a neutral tail, regardless of their initial velocity. The radiation pressure acceleration, for ions, is not computed here because it is negligible compared to the electromagnetic forces.

3. Model results: neutral and ionised tails of CoRoT-7b

In this study we concentrate on sodium and calcium, because it is possible to detect them by ground-based observation. Fig. 4 shows the sodium exospheric vertical profile; in Fig. 5 we show the tail of Na, as column density in the *xz*-plane, integrated along the *y* direction; the host star is on the right. The different plots refer to various model assumptions: top panel, thermal release from

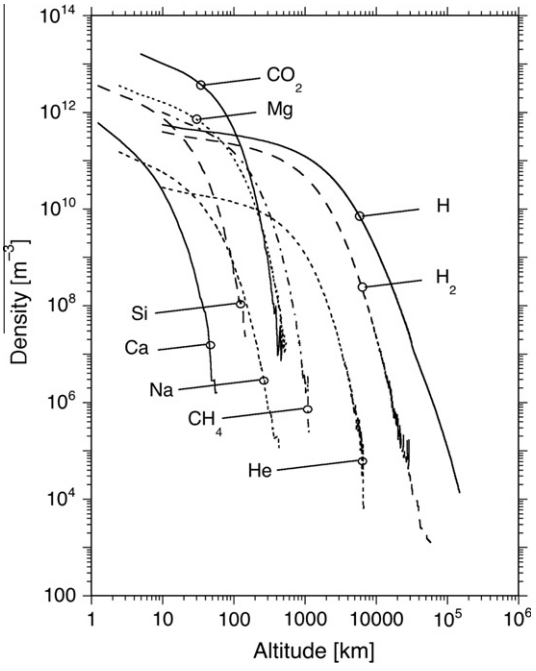

Fig. 4. Simulated vertical density profiles for an exobase temperature of 2500 K. Fluctuations at low particle densities are due to limited particle numbers in the simulation. Density profile for Mg is about 10 times higher than that of Ca.

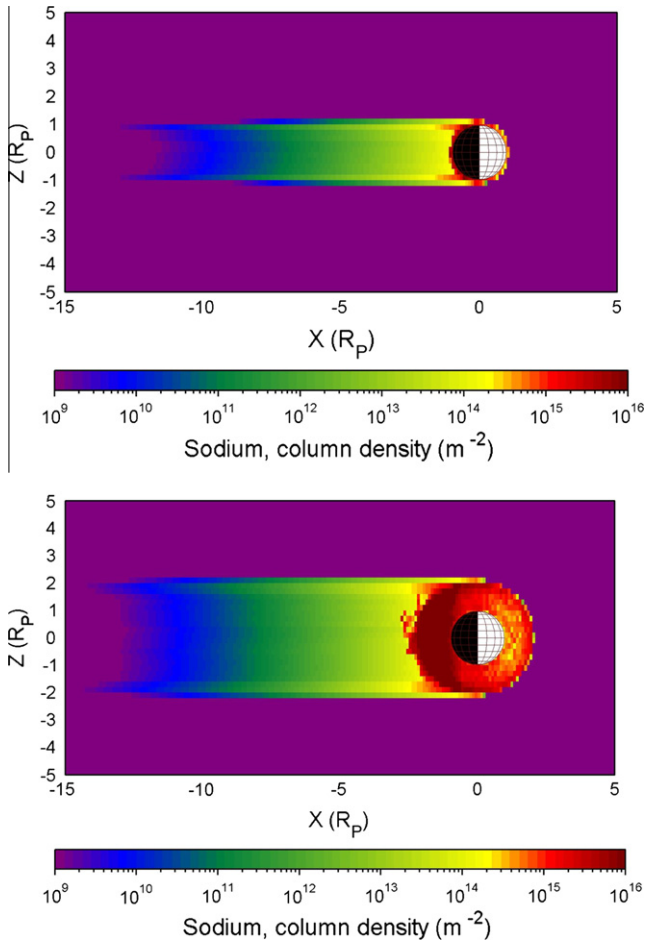

Fig. 5. Colour-coded map of the column density of Na, integrated along the *y* direction, in the reference frame of the planet. Host star is on the right. Top panel: thermal release from exobase at 200 km, temperature 2500 K; bottom panel: thermal release from exobase at 1 R_{pl}, temperature 10,000 K. The column density in the night side of the exosphere is higher due to the planetary shadowing effect. (For interpretation of the references to colour in this figure legend, the reader is referred to the web version of this article.)

the exobase at 200 km of height and 2500 K; bottom panel, thermal release from the exobase at 1 R_{pl} and 10,000 K. In all cases, the Na atoms are rapidly accelerated in the $-x$ direction by the radiation pressure and form a neutral tail behind the planet, in the planet reference frame. The acceleration by radiation pressure is huge (see Fig. 3), so that the tail is directed exactly towards the $-x$ direction; the non-inertial Coriolis force is almost negligible with respect to radiation pressure, and it just causes a small asymmetry in the *y* direction. If we look at the tail from the $-x$ direction, as in a transit observation, the tail has the same size of the planet and its atmosphere, in contrast to what is observed at Mercury, for example, where the tail can be twice as big as the planet (Schleicher et al., 2004).

In the case of an airless body, the precipitation of protons, approximately with an angle of 45° with respect to the *x*-axis, causes chemical sputtering of Na from the regolith, while the UV flux produces subsequent release from the surface (Mura et al., 2009). Once in the exosphere, Na particles are accelerated and form the sodium tail. Applying the same code already used at Mercury, and rescaling all parameters (photo-ionisation lifetime, radiation pressure acceleration, photon flux, stellar wind velocity and density) it is found that the overall Na density is a factor 10 higher than that estimated by the above models.

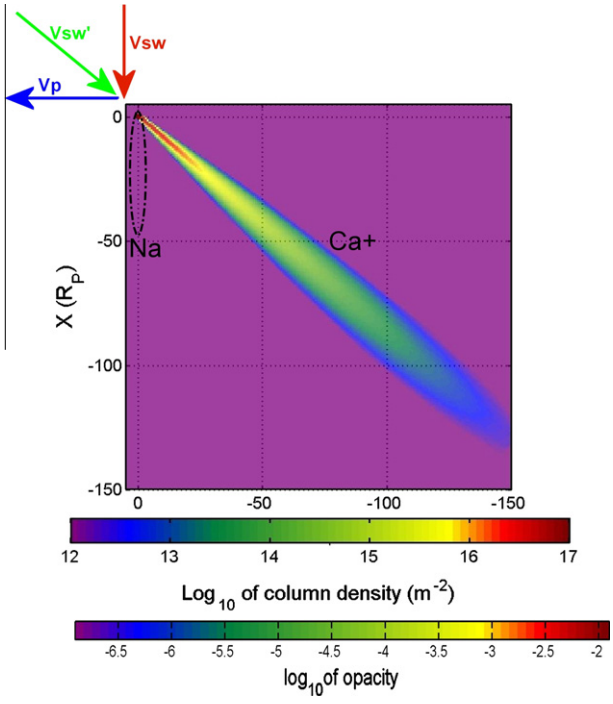

Fig. 6. Simulated Na and Ca^+ column densities in the *xy* plane, integrated along the *z* direction. The arrows indicate the velocity of the planet/reference frame (V_p), the velocity of the stellar wind in the inertial reference frame (V_{sw}) and in the non-inertial planetary reference frame (V'_{sw}). The Sodium tail is the narrow and short feature on the left (dashed line).

The photo-ionised Ca and Mg atoms are trapped in the interplanetary magnetic field and are dragged away from the planet, hence forming a Ca and Mg ion tail. In the reference frame of the planet, the tail is tilted of about 45° due to the stellar wind aberration. Fig. 6 shows the colour-coded density of Ca^+ ions in the *xy* plane, integrated along the *z* direction, in the case of the non-magnetised body. The Ca ion tail has a typical scale length of $v_{sw} \cdot \tau_{Ca+} = 10\ R_p$, when the Ca^+ ions become Ca^{++}. The Ca^+ density falls off exponentially and is still noticeable at about 100 R_p away from the planet. The Sodium tail is also plotted as a reference. Note that the two tails, the neutral Na and the ionised Ca tail, have different inclinations. Fig. 8 shows the colour-coded density of Mg^+ ions, in a similar way to Fig. 6.

The parameters that are used in the presented simulations refer to CoRoT-7b-like exoplanets, but some more general considerations may be done. As far as it concerns the Na tail, the planetary mass is not a critical parameter. In fact, in preliminary simulations we tried to use different planet masses (up to 10 M_{Earth}) without finding a significant difference in the Na tail density. This is because the main acting force on Na atoms is the radiation pressure (see Fig. 3). A larger planetary radius results in a larger Na tail cross section. The exobase temperature affects the velocity distribution of released particles; for a given exobase density, the thermal velocity it is linearly related to the Na flux from the exobase, and hence to the Na density in the tail. Simulations show that the global loss rate of sodium, is $Q_{Na} = 1.2 \times 10^{29}\ \mathrm{s}^{-1}$ for a 200 km high exobase at a temperature of $T = 1500$ K, and it increases to $Q_{Na} = 3.3 \times 10^{29}\ \mathrm{s}^{-1}$ at $T = 10{,}000$ K. The dependence is $Q_{Na} \sim \sqrt{T}$.

4. Feasibility of the observation of CoRoT-7b transiting exospheres

Here we discuss the feasibility of the observation of the planet and its coma during the transit of CoRoT-7b. Ca atoms were detected in the Ca I line in the exosphere and coma of Mercury (Bida et al., 2000; Killen et al., 2005) and Mercury's Na coma was detected on many occasions (see review Killen et al., 2007).

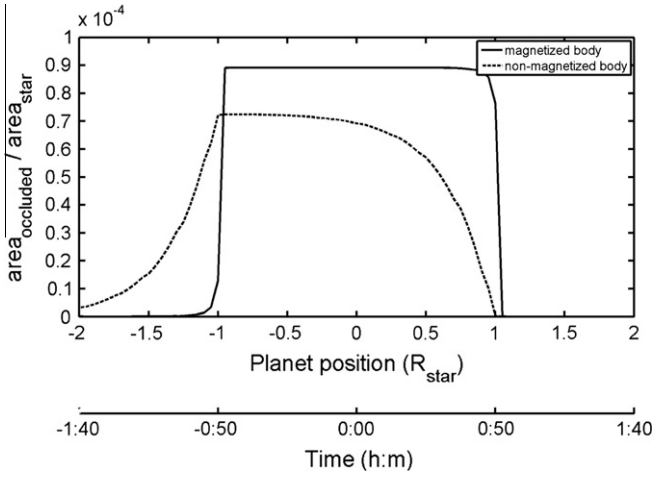

Fig. 7. Simulation of an occultation experiment: fraction of occluded area, due to Ca^+ absorption, function of the planet position with respect to the host star ($x = 0$ is the centre of the star). Time of observation is running from left to right.

The orbital velocity of the planet is about 200 km/s, and the transit of the planet lasts 1.3 h (Léger et al., 2009). During the transit, the Na tail will be along the direction of the observer, while the Ca^+ one will be at a 45° angle respect to the star-observer direction. Such Ca^+ population will be able to absorb the star spectrum in the Ca^+ absorption lines. The absorptivity *A* can be calculated as:

$$A = 1 - e^{(-d\sigma)} \tag{7}$$

where *d* is the column density of Ca^+ and σ is the cross section (1.2×10^{-15} cm^2, Ca II K and H lines, at 3933 and 3968 Å). The result is shown in Fig. 6 (bottom colour scale). Note that the scale length in the *y* direction is just $v_{\mathrm{planet}}\tau_{Ca}$, and the velocity of the stellar wind does not affect the shape of the tail in the *xz*-plane, and hence our estimation of the absorptivity.

The most promising ion likely to be detectable in the coma by spectroscopy of transits is Ca^+ because of the short ionisation time of Ca atoms. Mg^+ is also a good candidate because of its likely higher abundance in the surface, thus also in the exosphere, and reasonably short ionisation time and low radiation pressure (McClintock et al., 2009). From our model calculations we expect that the exosphere leads to a very elongated Ca^+ coma (up to 100 $R_p = 2\ R_{\mathrm{star}}$ with a width up to 5–7 R_p). According to our model, if the planet is magnetised (with $r_{so} \approx 1.5\ R_p$) the coma is narrower. As the planet transit is progressing, the surface covered by the coma increases with time up to its maximum value of the order of magnitude of R_p^2. The resulting value of the transit depth at its maximum *P* when the leading planet is egressing is $\approx(1/\pi)\ (R_P/R_{\mathrm{star}})^2 \approx 1 \times 10^{-4}$. When the planet has egressed the stellar disk, the Ca^+ coma is still transiting the star, with an opacity decreasing with a time scale $\approx$1 h. From the line depth variation with time we will extract the column density along the coma.

Fig. 7 shows the absorption due to the presence of Ca^+, expressed as a fraction of the whole star photon flux in the Ca^+ absorption lines. Note that the total amount of Ca^+ is roughly the same in both magnetospheric configurations, since it is equal to the global Ca^+ production rate multiplied by its lifetime. However, the time profile of the absorption is different in the two cases, depending on the spatial distribution of Ca^+. This shows how it is possible to obtain basic information about the magnetisation state of the planet from the observation of the Ca^+ opacity versus time during the transit.

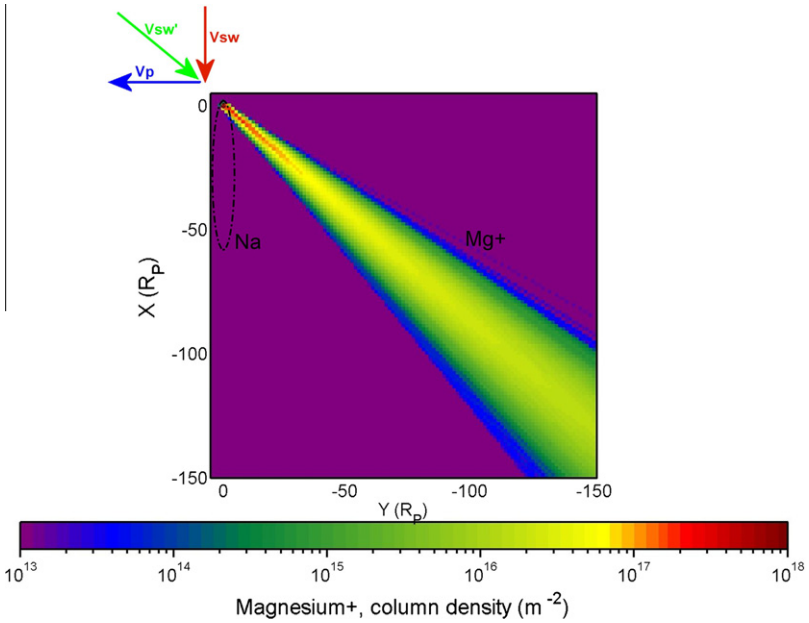

Fig. 8. Simulated Mg^+ column density in the *xy* plane, integrated along the *z* direction. Coordinate system similar to Fig. 6. The Sodium tail is the narrow and short feature on the left (dashed line).

The second promising element for observation during transit is Na. However, since the Na tail is radial, i.e., it is aligned with the line-of-sight during transit, its cross section is small and it is probably more difficult to detect such a tail.

To record high signal-to-noise-ratio spectra of the exosphere also out of transit spectra from the same night will be required. Hence, the observations should start 1 h before the transit and be continued 1 or 2 h after the transit of the planetary disk. Since the transit of the exosphere and the planet takes 3 h, this will result in an observing time of about 5–6 h. The total opaque area, with the parameters used here, is of the same order of magnitude as the planetary area. Since such a detection may be difficult to achieve by ground-based observations, similar investigations may be done using different ion species: for example, the density of Mg^+ is expected to be at least 10 times higher than that of Ca^+, because the density of Mg at the exosphere is higher (6×10^{12} m^{-3}) and because the ionisation lifetime is about 500 s. The density of Mg^+ in the tail of a CoRoT-7b-like planet, in the case of an unmagnetised body, is shown in Fig. 8. The possibility of detecting such exospheres by space telescopes may be investigated as well.

5. Summary and conclusions

In this study we present simulations about exospheric features of the CoRoT-7b planet that can be observed from ground. Different exospheric models are applied; however, some considerations and conclusions are valid for all models. A sodium neutral atom tail is likely to form behind the planet resulting from the enormous amount of the radiation pressure acceleration. Such a tail extends from the planet in the anti-sunward direction, and, even if the density would be high as calculated the configuration is not optimal for transit observation because the tail is aligned with the line-of-sight during observations.

Any ion population filling the magnetotail, and, in general, any ionised tail, such as calcium ions, would be aligned at an angle equal to the stellar wind aberration (cf. cometary ion tails). Since the orbital velocity is similar to the stellar wind velocity, it is expected that the magnetotail will form an angle of about 45° with the star–planet direction, which leads to a longer transit duration. The total amount of Ca^+ in the tail depends only on the global emission rate and the photo-ionisation lifetime of Ca^+. On the other hand, the opacity is a non-linear function of the column density, and it also depends on the spatial distribution of the Ca^+, which is related to the magnetospheric configuration, because we expect the Ca^+ to be confined inside the magnetosphere of the planet. Hence, the observation of Ca^+ would give us important information about CoRoT-7b magnetosphere and thus of a possible global magnetic field of CoRoT-7b. More generally, we would gain information on the interior of super-Earth planets and magnetic dynamo generation, about the universality of magnetic dynamo process and of magnetic moment scaling laws.

The observation of sodium atoms and calcium and magnesium ions in the exosphere of CoRoT-7b would prove that the exospheres of the rocky planets in our Solar System are not unique but a common feature amongst the rocky planets outside the Solar System. Moreover, this project would be the very first attempt to learn something of the mineralogy of a rocky planet orbiting another star. The detection of Na in the giant planets HD 209458b and HD 198733b using ground-based telescopes (Redfield et al., 2008; Snellen et al., 2008) is encouraging, and shows that the project is feasible if the exosphere is dense enough.

Acknowledgments

H. Lammer, M.L. Khodachenko, H. Rauer, A. Erikson and Ph. von Paris acknowledge support from the Helmholtz-Gemeinschaft as this research has been supported by the Helmholtz-Gemeinschaft through the research alliance "Planetary Evolution and Life". The authors also acknowledge the International Space Science Institute (ISSI; Bern, Switzerland) and the ISSI teams "Evolution of Habitable Planets" and "Evolution of Exoplanet Atmospheres and their Characterization". A. Mura, M.L. Khodachenko and H. Lammer acknowledge also support from the Europlanet Na 2 Wg 4 and Wg 5.

References

Adams, E., Seager, S., Elkins-Tanton, L., 2008. Ocean planet or thick atmosphere: On the mass–radius relationship for solid exoplanets with massive atmospheres. Astrophys. J. 673, 1160–1164.

Barnes, R., Raymond, S.N., Greenberg, R., Jackson, B., Kaib, N.A., 2010. CoRoT-7b: Super-Earth or Super-Io? Astrophys. J. 709 (2), L95. doi:10.1088/2041-8205/709/2/L95.

Bida, T.A., Killen, R.M., Morgan, T.H., 2000. Discovery of calcium in Mercury's atmosphere. Nature 404, 159–161.
Bzowski, M., 2008. Survival probability and energy modification of hydrogen energetic neutral atoms on their way from the termination shock to Earth orbit. Astron. Astrophys. 488, 1057–1068.
Christensen, U.R., Aubert, J., 2006. Scaling properties of convection-driven dynamos in rotating spherical shells and application to planetary magnetic fields. Geophys. J. Int. 166, 97–114.
Delcourt, D.C., Grimald, S., Leblanc, F., Berthelier, J.-J., Millilo, A., Mura, A., Orsini, S., Moore, T.E., 2003. A quantitative model of the planetary Na+ contribution to Mercury's magnetosphere. Ann. Geophys. 21, 1723.
Fegley, B., Cameron, A.G.W., 1987. A vaporization model for iron/silicate fractionation in the Mercury protoplanet, Earth Planet. Sci. Lett. 82, 207–222.
Fulle, M., Leblanc, F., Harrison, R.A., Davis, C.J., Eyles, C.J., Halain, J.P., Howard, R.A., Bockelée-Morvan, D., Cremonese, G., Scarmato, T., 2007. Discovery of the atomic iron tail of Comet McNaught using the Heliospheric Imager on STEREO. Astrophys. J. 661, L93–L96.
Gladman, B., Quinn, D., Nicholson Philip, D., Rand, R., 1996. Synchronous locking of tidally evolving satellites. Icarus 122, 166–192.
Grasset, O., Schneider, J., Sotin, C., 2009. A study of the accuracy of mass–radius relationships for silicate-rich and ice-rich planets up to 100 Earth masses. Astrophys. J. 693, 722–733.
Grießmeier, J.-M., Stadelmann, A., Motschmann, U., Belisheva, N.K., Lammer, H., Penz, T., 2005. Cosmic ray impact on extrasolar Earth-like planets in close-in habitable zones. Astrobiology 5 (5), 587–603.
Grießmeier, J.-M., Stadelmann, A., Grenfell, J.L., Lammer, H., Motschmann, U., 2009. On the protection of extrasolar Earth-like planets around K/M stars against galactic cosmic rays. Icarus 199 (2), 526–535.
Huebner, W.F., Keady, J.J., Lyon, S.P., 1992. Solar photo rates for planetary atmospheres and atmospheric pollutants. Astrophys. Space Sci. 195, 1–294.
Ip, W.-H., 1986. The sodium exosphere and magnetosphere of Mercury. Geophys. Res. Lett. 13, 423–426.
Johnson, R.E., 1990. Energetic Charged Particle Interactions with Atmospheres and Surfaces. Springer, Berlin, Heidelberg, New York.
Khodachenko, M.L. et al., 2007. CME activity of low mass M stars as an important factor for the habitability of terrestrial exoplanets Part I: CME impact on expected magnetospheres of Earth-like exoplanets in close-in habitable zones. Astrobiology 7, 167–184.
Killen, R.M., Ip, W.-H., 1999. The surface-bounded atmospheres of Mercury and the Moon. Rev. Geophys. 37, 361–406.
Killen, R.M., Bida, T.A., Morgan, T.H., 2005. The calcium exosphere of Mercury. Icarus 173, 300–311.
Killen, R. et al., 2007. Processes that promote and deplete the exosphere of Mercury. Space Sci. Rev. 132, 433–509.
Kulikov, Yu.N. et al., 2006. Atmospheric and water loss from early Venus. Planet. Space Sci. 54, 1425–1444.
Lammer, H., Bauer, S.J., 1993. Atmospheric mass loss from Titan by sputtering. Planet. Space Sci. 41, 657–663.
Lammer, H. et al., 2009. Determining the mass loss limit for close-in exoplanets: What can we learn from transit observations? Astron. Astrophys. 506, 399–410.
Léger, A. et al., 2009. Transiting exoplanets from the CoRoT space mission VIII. CoRoT-7b: The first super-Earth with measured radius. Astron. Astrophys. 506 (1), 287–302.
Leitzinger, M., Odert, P., Lammer, H., Kulikov, Yu.N., Khodachenko, M.L., Weingrill, J., Hanslmeier, A., Biernat, H.K., Schneider, J., 2009. Could CoRoT-7b be a remnant of an evaporated gas or ice giant? Planet. Space Sci., submitted for publication.
McClintock, W.E., Vervack Jr., R.J., Bradley, E.T., Killen, R.M., Mouawad, N., Sprague, A.L., Burger, M.H., Solomon, S.C., Izenberg, N.R., 2009. MESSENGER observations of Mercury's exosphere: Detection of magnesium and distribution of constituents. Science 324 (5927), 597–598.
Mura, A., Milillo, A., Orsini, S., Massetti, S., 2007. Numerical and analytical model of Mercury's exosphere: Dependence on surface and external conditions. Planet. Space Sci. 55, 1569–1583.
Mura, A., Wurz, P., Lichtenegger, H.I.M., Schleicher, H., Lammer, H., Delcourt, D., Milillo, A., Orsini, S., Massetti, S., Khodachenko, M.L., 2009. The sodium exosphere of Mercury: Comparison between observations during Mercury's transit and model results. Icarus 200, 1–11.
O'Neill, C., Jellinek, A.M., Lenardic, A., 2007. Conditions for the onset of plate tectonics on terrestrial planets and moons. Earth Planet. Sci. Lett. 261, 20–32.
Penz, T. et al., 2008. Mass loss from "Hot Jupiters"—Implications for CoRoT discoveries. Part II: Long time thermal atmospheric evaporation modeling. Planet. Space Sci. 56, 1260–1273.
Potter, A., Killen, R.M., Morgan, T.H., 2002. The sodium tail of Mercury. Meteor. Planet. Sci. 37 (9), 1165–1172.
Queloz, D. et al., 2009. The CoRoT-7 planetary system: Two orbiting super-Earths. Astron. Astrophys. 506 (1), 303–319.
Redfield, S., Endl, M., Cochran, W.D., Koesterke, L., 2008. Sodium absorption from the exoplanetary atmosphere of HD 189733b detected in the optical transmission spectrum. Astrophys. J. 673, L87–L90.
Schaefer, L., Fegley Jr., B., 2009. Chemistry of silicate atmospheres of evaporating super-Earths. Astrophys. J. 703, L113–L117.
Schleicher, H., Wiedemann, G., Wöhl, H., Berkefeld, T., Soltau, D., 2004. Detection of neutral sodium above Mercury during the transit on 2003 May 7. Astron. Astrophys. 425, 1119–1124.
Schneider, J., Rauer, H., Lasota, J.-P., Bonazzola, S., Chesefière, E., 1998. The cometary tail of giant extrasolar planets at small orbital distance. In: Rebolo, Rafael, Martin, Eduardo L., Zapatero Osorio, Maria Rosa (Eds.), Brown Dwarfs and Extrasolar Planets, ASP Conference Series, vol. 134, p. 241–244.
Smyth, W.H., Marconi, M.L., 1995. Theoretical overview and modeling of the sodium and potassium atmospheres of Mercury. Astrophys. J. 441, 839–864.
Snellen, I.A.G., Albrecht, S., de Mooij, E.J.W., Le Poole, R.S., 2008. Ground-based detection of sodium in the transmission spectrum of exoplanet HD 209458b. Astron. Astrophys. 487 (1), 357–362.
Tian, F., Kasting, J.F., Liu, H.-L., Roble, R.G., 2009. Hydrodynamic planetary thermosphere model: 1. Response of the Earth's thermosphere to extreme solar EUV conditions and the significance of adiabatic cooling. J. Geophys. Res. 113 (E5) (CiteID E0500).
Tinetti, G. et al., 2007. Water vapour in the atmosphere of an extrasolar planet water vapour in the atmosphere of a transiting extrasolar planet. Nature 448, 169–171.
Valencia, D., O'Connell, R.J., Sasselov, D.D., 2007. Inevitability of plate tectonics on super-Earths. Astrophys. J. 670, L45–L48.
Walker, R.J., Russel, C.T., 1995. In: Kivelson, M.G., Russell, C.T. (Eds.), Introduction to Space Physics. Cambridge Univ. Press, New York, pp. 227–287.
Wurz, P., Lammer, H., 2003. Monte-Carlo simulation of Mercury's exosphere. Icarus 164 (1), 1–13.
Wurz, P., Rohner, U., Whitby, J.A., Kolb, C., Lammer, H., Dobnikar, P., Martín-Fernández, J.A., 2007. The lunar exosphere: The sputtering contribution. Icarus 191, 486–496.
Wurz, P., Whitby, J.A., Rohner, U., Martín-Fernández, J.A., Lammer, H., Kolb, C., 2010. The contribution to Mercury's exosphere by sputtering, micrometeorite impact and photon-stimulated desorption. Planet. Space Sci., in press, doi:10.1016/j.pss.2010.08.003.